Hierarchical one-dimensional finite elements for the thermal stress analysis of three-dimensional functionally graded beams

Hierarchical one-dimensional finite elements for the thermal stress analysis of three-dimensional functionally graded beams

G. De Pietro[*],
Luxembourg Institute of Science and Technology,
5, avenue des Hauts-Fourneaux, L-4362 Esch-sur-Alzette, Luxembourg and
Politecnico di Torino, c.so Duca degli Abruzzi 24, 10129 Turin, Italy

Y. Hui [†],
Luxembourg Institute of Science and Technology,
5, avenue des Hauts-Fourneaux, L-4362 Esch-sur-Alzette, Luxembourg and
Politecnico di Torino, c.so Duca degli Abruzzi 24, 10129 Turin, Italy and
School of Civil Engineering, Wuhan University,
8 South Road of East Lake, 430072 Wuhan, PR China

G. Giunta[‡], S. Belouettar[§],
Luxembourg Institute of Science and Technology,
5, avenue des Hauts-Fourneaux, L-4362 Esch-sur-Alzette, Luxembourg

E. Carrera[¶],
Politecnico di Torino,
c.so Duca degli Abruzzi 24, 10129 Turin, Italy

H. Hu[‖],
School of Civil Engineering, Wuhan University,
8 South Road of East Lake, 430072 Wuhan, PR China

Author for correspondence:
Gabriele De Pietro, Ph.D. student,
Materials Research and Technology Department,
Luxembourg Institute of Science and Technology,
5, avenue des Hauts-Fourneaux,
L-4362 Esch-sur-Alzette, Luxembourg.
tel: +352 275 888 1,
fax: +352 275 885,
e-mail: gabriele.depietro@list.lu

[*]Ph.D. student.
[†]Ph.D. student.
[‡]Research scientist.
[§]Research Scientist.
[¶]Full Professor.
[‖]Full Professor.

Abstract

In this work, the thermoelastic response of functionally graded beams is studied. To this end, a family of advanced one-dimensional finite elements is derived by means of a unified formulation that is not dependent on the order of approximation of the displacements upon the beam cross-section. The temperature field is obtained via a Navier-type solution of Fourier's heat conduction equation and it is considered as an external load within the mechanical analysis. The stiffness matrix of the elements is derived via the Principle of Virtual Displacements. Numerical results in terms of temperature, displacements and stresses distribution are provided for different beam slenderness ratios and type of material gradation. Linear, quadratic and cubic elements are used. Results are validated through comparison with three-dimensional finite elements solutions obtained by the commercial software ANSYS. It is shown that accurate results can be obtained with reduced computational costs.

Keywords: thermal loads, beam structures, functionally graded materials, hierarchical modelling, one-dimensional finite elements.

1 Introduction

Functionally Graded Materials (FGMs) are generally used in structural components operating in extremely high temperature environments. They are characterised by high temperature resistances and smooth stress distributions thanks to a gradual variation of the volume fraction of the constituent materials.

Many studies on FGM beams under mechanical or thermal loads are available in the literature. An overview of recent works about thermo-mechanical analyses and functionally graded structures follows. Thermo-elasticity problems were discussed in the book by Hetnarski and Eslami [1], where thermal stress analyses of Euler-Bernoulli beams made of functionally graded materials can also be found. Noda [2] investigated the optimal gradation laws to minimize thermal stresses in FGM structures. A finite element solution based on Thimoshenko's beam theory was developed by Chakraborty et al. [3], accounting for an exponential and a power law variation of material properties through the thickness. Analytical solutions for the thermo-elastic stress analysis of multi-layered functionally graded Euler-Bernoulli beams were given by Carpinteri and Paggi [4]. Wang and Qin [5] presented a meshless method for the thermo-elastic analysis of FGM structures combined with radial basis functions. The free vibration of FGM beams subjected to initial thermal stress was studied by Mahi et al. [6]. The temperature field was obtained solving a one-dimensional steady-state heat conduction equation. Several shear deformation theories were investigated. Wattanasakulpong et al. [7] carried out thermo-elastic vibration and thermal buckling analyses of FGM beams by means of a third-order shear deformation theory. Material properties were considered to be dependent on the temperature via a non-linear polynomial law [8]. Xiang et al. [9] investigated the free and forced vibration of a functionally graded beam under thermally induced initial stresses assuming Timoshenko's kinematic hypotheses. Sankar and Tzeng [10] presented a closed-form solution of the thermoelastic equilibrium equations for a functionally graded beam by Euler-Bernoulli's model. The thermoelastic properties of the material and the temperature were assumed to vary exponentially through the thickness. Sankar [11] obtained an elasticity solution for a functionally graded Euler-Bernoulli beam subjected to trasverse loads. Lezgy-Nazargah [12] studied bi-directional FGM beams under thermal stresses. The displacement field was assumed as the combination of polynomials and exponential functions. The temperature field was approximated by a Hermite interpolation along the thickness direction. As far as the axial variation is concerned, non-uniform rational basis-spline functions were used. The governing equations were obtained from the principle of stationary potential energy. Kiani and Eslami [13] analysed the buckling of Euler-Bernoulli beams under various types of thermal loading. A power law across the thickness of the beam was considered. Nonlinear strain-displacement relations were assumed. A closed form solution for the critical buckling temperature was obtained. Zhang [14] used a physical neutral surface theory and a high-order shear deformation model for the bending analysis of functionally graded beams. Nonlinear von Kármán strain-displacement relationships were considered. The material properties were assumed to be temperature dependent and to vary along the thickness. Ritz method was used in order to obtain a nonlinear bending approximate solution. Kocaturk and Akbas [15] carried out a post-buckling analysis of functionally graded Timoshenko beams under thermal loading considering full geometric non-linearity via the finite element method. Sun et al. [16] used the shooting method to investigate the buckling and post-buckling deformations of a functionally graded material Timoshenko beam subjected to a temperature rise and resting on a two-parameter non-linear elastic foundation. Through-the-thickness temperature distribution was deter-

mined by numerically solving the one-dimensional heat conduction equation. Geometric non-linearities in the strain-displacement relations were accounted for.

A thermal stress analysis of functionally graded beams via advanced one-dimensional finite elements is addressed in this paper. The stiffness matrix of the element is derived via a Unified Formulation (UF) that was previously proposed for plates and shells, (see Carrera [17]) and extended to beams (see Carrera et al. [18], Giunta et al. [19] [20] [21] [22] and Catapano et al. [23]). UF has been recently employed for thermal stress analyses of composite beams in the framework of strong form solutions and finite elements method applied to isotropic and laminated beams (see Giunta et al. [24] [25] [26]). The novelty of the present work consists in the use of the finite element method to solve, in a weak sense, the governing differential equations governing the response of a FGM three-dimensional beam under thermal loads. Shear locking phenomenon is avoided by a classical selective integration procedure that is effective regardless the approximation order over the cross-section. In the proposed UF, the displacements' polynomial approximation over the beam cross-section is written in a compact form. The stiffness matrix of the element is derived through the Principle of Virtual Displacements in terms of a fundamental nucleus, which is unique regardless the displacement approximation order as well as the number of nodes per element. Numerical investigations are carried out considering a power law variation along the beam thickness direction of the elastic and thermal material properties. Slender and deep beams are investigated with both simply supported and cantilever boundary conditions. Results are provided in terms of temperature, displacements and stresses. A three-dimensional finite elements solution provided by the commercial software ANSYS is used for validation.

2 Preliminaries

A beam is a structure whose axial extension (l) is predominant if compared to any other dimension orthogonal to it. The cross-section is identified by intersecting the beam with a plane orthogonal to its axis. A Cartesian reference system is adopted, see Fig. 1. The x axis is aligned with the direction of the longitudinal axis of the beam and it is bounded such that $0 \leq x \leq l$. y- and z-axis are two orthogonal directions laying on the cross-section, which is considered to be constant along x. The displacement vector is:

$$\mathbf{u}^T(x,y,z) = \left\{ \begin{array}{ccc} u_x(x,y,z) & u_y(x,y,z) & u_z(x,y,z) \end{array} \right\} \tag{1}$$

where u_x, u_y and u_z are the displacement components. Superscript 'T' represents the transposition operator. Stress vector $\boldsymbol{\sigma}$ and strain vector $\boldsymbol{\varepsilon}$ are grouped into a part relative to the cross-section ($\boldsymbol{\sigma}_n$, $\boldsymbol{\varepsilon}_n$) and a part relative to planes orthogonal to the cross-section ($\boldsymbol{\sigma}_p$, $\boldsymbol{\varepsilon}_p$):

$$\boldsymbol{\sigma}_n^T = \left\{ \begin{array}{ccc} \sigma_{xx} & \sigma_{xy} & \sigma_{xz} \end{array} \right\} \quad \boldsymbol{\sigma}_p^T = \left\{ \begin{array}{ccc} \sigma_{yy} & \sigma_{zz} & \sigma_{yz} \end{array} \right\} \tag{2}$$

$$\boldsymbol{\varepsilon}_n^T = \left\{ \begin{array}{ccc} \varepsilon_{xx} & \varepsilon_{xy} & \varepsilon_{xz} \end{array} \right\} \quad \boldsymbol{\varepsilon}_p^T = \left\{ \begin{array}{ccc} \varepsilon_{yy} & \varepsilon_{zz} & \varepsilon_{yz} \end{array} \right\} \tag{3}$$

Under the hypothesis of geometric linearity, strain-displacement relations in vectorial notation are given by:

$$\begin{array}{c} \boldsymbol{\varepsilon}_n = \mathbf{D}_{np}\mathbf{u} + \mathbf{D}_{nx}\mathbf{u} \\ \boldsymbol{\varepsilon}_p = \mathbf{D}_p\mathbf{u} \end{array} \tag{4}$$

where $\mathbf{D}_{np}$, $\mathbf{D}_{nx}$ and $\mathbf{D}_p$ are the following differential matrix operators:

$$\mathbf{D}_{np} = \begin{bmatrix} 0 & 0 & 0 \\ \dfrac{\partial}{\partial y} & 0 & 0 \\ \dfrac{\partial}{\partial z} & 0 & 0 \end{bmatrix} \quad \mathbf{D}_{nx} = \mathbf{I}\frac{\partial}{\partial x} \quad \mathbf{D}_p = \begin{bmatrix} 0 & \dfrac{\partial}{\partial y} & 0 \\ 0 & 0 & \dfrac{\partial}{\partial z} \\ 0 & \dfrac{\partial}{\partial z} & \dfrac{\partial}{\partial y} \end{bmatrix} \tag{5}$$

and $\mathbf{I}$ is the unit matrix.

The constitutive equations in the case of a thermo-mechanical problem are given by:

$$\begin{aligned} \boldsymbol{\sigma}_p &= \boldsymbol{\sigma}_{pe} - \boldsymbol{\sigma}_{pt} = \mathbf{C}_{pp}\boldsymbol{\varepsilon}_p + \mathbf{C}_{pn}\boldsymbol{\varepsilon}_n - \lambda_p T \\ \boldsymbol{\sigma}_n &= \boldsymbol{\sigma}_{ne} - \boldsymbol{\sigma}_{nt} = \mathbf{C}_{np}\boldsymbol{\varepsilon}_p + \mathbf{C}_{nn}\boldsymbol{\varepsilon}_n - \lambda_n T \end{aligned} \tag{6}$$

where subscripts 'e' and 't' refer to the elastic and the thermal contributions, respectively. For isotropic materials, the matrices $\mathbf{C}_{pp}$, $\mathbf{C}_{pn}$, $\mathbf{C}_{np}$ and $\mathbf{C}_{nn}$ in Eqs. 6 are in the following form:

$$\mathbf{C}_{pp} = \begin{bmatrix} C_{22} & C_{23} & 0 \\ C_{23} & C_{33} & 0 \\ 0 & 0 & C_{44} \end{bmatrix} \quad \mathbf{C}_{pn} = \mathbf{C}_{np}^T = \begin{bmatrix} C_{12} & 0 & 0 \\ C_{13} & 0 & 0 \\ 0 & 0 & 0 \end{bmatrix} \quad \mathbf{C}_{nn} = \begin{bmatrix} C_{11} & 0 & 0 \\ 0 & C_{66} & 0 \\ 0 & 0 & C_{55} \end{bmatrix} \tag{7}$$

The coefficients C_{ij} are given by:

$$\begin{gathered} C_{11} = C_{22} = C_{33} = \frac{1-\nu}{(1+\nu)(1-2\nu)}E \quad C_{12} = C_{13} = C_{23} = \frac{\nu}{(1+\nu)(1-2\nu)}E \\ C_{44} = C_{55} = C_{66} = \frac{1}{2(1+\nu)}E \end{gathered} \tag{8}$$

in which Young's modulus (E) and Poisson's ratio (ν) are function of the cross-section coordinates. The coefficients λ_n and λ_p:

$$\boldsymbol{\lambda}_n^T = \left\{ \begin{array}{ccc} \lambda_1 & 0 & 0 \end{array} \right\} \quad \boldsymbol{\lambda}_p^T = \left\{ \begin{array}{ccc} \lambda_2 & \lambda_3 & 0 \end{array} \right\} \tag{9}$$

are related to the thermal expansion coefficients α_n and α_p:

$$\boldsymbol{\alpha}_n^T = \left\{ \begin{array}{ccc} \alpha_1 & 0 & 0 \end{array} \right\} \quad \boldsymbol{\alpha}_p^T = \left\{ \begin{array}{ccc} \alpha_2 & \alpha_3 & 0 \end{array} \right\} \tag{10}$$

through the following equations:

$$\begin{aligned} \boldsymbol{\lambda}_p &= \mathbf{C}_{pp}\boldsymbol{\alpha}_p + \mathbf{C}_{pn}\boldsymbol{\alpha}_n \\ \boldsymbol{\lambda}_n &= \mathbf{C}_{np}\boldsymbol{\alpha}_p + \mathbf{C}_{nn}\boldsymbol{\alpha}_n \end{aligned} \tag{11}$$

In order to have a general software implementation not depending upon a specific gradation law of the FGM, a Lagrange approximation on N_p Chebyshev points along y and z cross-section coordinates based on Newton series expansion is assumed for the material stiffness coefficients C_{ij} and thermal coefficients λ_i:

$$\begin{aligned} C_{ij}(y,z) &\approx \omega_\xi(y)\,\omega_\eta(z)\,C_{ij}[y_0,\ y_1,\ \ldots,\ y_\xi; z_0,\ z_1,\ \ldots,\ z_\eta] \\ \lambda_i(y,z) &\approx \omega_\xi(y)\,\omega_\eta(z)\,\lambda_i[y_0,\ y_1,\ \ldots,\ y_\xi; z_0,\ z_1,\ \ldots,\ z_\eta] \end{aligned} \quad \text{with} \quad \xi,\eta = 0,\ 1,\ \ldots,\ N_p \tag{12}$$

being:

$$\omega_m(\zeta) = \begin{cases} 1 & m = 0 \\ \displaystyle\prod_{n=0}^{m-1}(\zeta - \zeta_n) & m \in [1, N_p] \end{cases} \tag{13}$$

and $C_{ij}[\ldots;\ldots]$ and $\lambda_i[\ldots;\ldots]$ the divided difference of the approximated function, see Philips [27]. Chebyshev's points are defined on the domain $[-1,+1]$ via the following equation:

$$\zeta_m = \cos\left(\frac{m\pi}{N_p}\right) \quad \text{with} \quad m = 0,\ 1,\ \ldots,\ N_p \tag{14}$$

The natural coordinates of these points are then transformed into the cross-section coordinates via a variable transformation. Through this procedure, the software implementation of the proposed models does not depend upon a specific gradation law that, once defined, will be approximated via a Newton series expansion.
Temperature (T) is treated as an external load resulting in the internal thermal stresses. Fourier's heat conduction equation is analytically solved to obtain the temperature profile over the whole domain of the beam. The following multiplicative variable separation is used:

$$T(x,y,z) = \Theta_n(x)\,\Theta_\Omega(y,z) \tag{15}$$

where $\Theta_n(x)$ is a sinusoidal function along the beam axis direction and $\Theta_\Omega(y,z)$ an exponential function of the cross-section coordinates. The solution procedure is presented in the Appendix.

3 Displacement Field Approximation

The variation of the displacement upon the cross-section is postulated a-priori. Several displacement-based beam theories can be formulated on the basis of the following generic kinematic field:

$$\mathbf{u}(x,y,z) = F_\tau(y,z)\,\mathbf{u}_\tau(x) \quad \text{with} \quad \tau = 1,\ 2,\ \ldots,\ N_u \tag{16}$$

According to Einstein's notation, subscript τ implicitly represents a summation. $F_\tau(y,z)$ is a generic function of the cross-section coordinates and N_u is the number of terms accounted in the summation.
In this study, Mac Laurin's polynomials are used as approximating functions $F_\tau(y,z)$. The choice of F_τ as well as N_u is arbitrary. N_u and F_τ as function of the order of the approximating polynomials N are shown in Pascal's triangle in Table 1.
The explicit form of a generic N-order displacement field reads:

$$\begin{aligned}
u_x &= u_{x1} + u_{x2}y + u_{x3}z + \cdots + u_{x\frac{(N^2+N+2)}{2}}y^N + \cdots + u_{x\frac{(N+1)(N+2)}{2}}z^N,\\
u_y &= u_{y1} + u_{y2}y + u_{y3}z + \cdots + u_{y\frac{(N^2+N+2)}{2}}y^N + \cdots + u_{y\frac{(N+1)(N+2)}{2}}z^N,\\
u_z &= u_{z1} + u_{z2}y + u_{z3}z + \cdots + u_{z\frac{(N^2+N+2)}{2}}y^N + \cdots + u_{z\frac{(N+1)(N+2)}{2}}z^N.
\end{aligned} \tag{17}$$

The displacement variation along the beam axis is approximated via finite element method:

$$\mathbf{u}(x,y,z) = F_\tau(y,z)\,N_i(x)\,\mathbf{q_{\tau i}} \quad \text{with} \quad \tau = 1,\ 2,\ \ldots,\ N_u \quad \text{and} \quad i = 1,\ 2,\ \ldots,\ N_n^e \tag{18}$$

$N_i(x)$ is a C^0 Lagrangian shape function, N_n^e the number of nodes per element and $\mathbf{q_{\tau i}}$ the unknown nodal displacement vector. Linear, quadratic and cubic elements are used and they are referred to as "B2", "B3" and "B4", respectively.

4 Element Stiffness Matrix

The stiffness matrix of the element is obtained via the Principle of Virtual Displacements (PVD) for a static thermo-elastic analysis:

$$\delta L_{\text{int}} = 0 \tag{19}$$

L_{int} represents the strain energy and δ stands for a virtual variation. According to the stress and strain vectors splitting in Eqs. 2 and 3, the virtual variation of the strain energy is:

$$\delta L_{\text{int}} = \int_{l_e}\int_{\Omega} \left(\delta\boldsymbol{\epsilon}_{tn}^T\boldsymbol{\sigma}_n + \delta\boldsymbol{\epsilon}_{tp}^T\boldsymbol{\sigma}_p\right) d\Omega dx. \tag{20}$$

where l_e is the element length and Ω the cross-section. If geometrical relations in Eqs. 4, constitutive relations in Eqs. 6 and finite element formulation in Eq. 18 are considered, Eq. 20 reads:

$$\begin{aligned}\delta L_{\text{int}} = \quad & \delta\mathbf{q}_{\tau i}^T \int_{l_e}\int_{\Omega} \Big\{ \left(\mathbf{D}_{nx}N_i\right)^T F_\tau \left[\mathbf{C}_{np}\left(\mathbf{D}_p F_s\right) N_j + \mathbf{C}_{nn}\left(\mathbf{D}_{np}F_s\right) N_j + \mathbf{C}_{nn}F_s\left(\mathbf{D}_{nx}N_j\right)\right] \\ & + \left(\mathbf{D}_{np}F_\tau\right)^T N_i \left[\mathbf{C}_{np}\left(\mathbf{D}_p F_s\right) N_j + \mathbf{C}_{nn}\left(\mathbf{D}_{np}F_s\right) N_j + \mathbf{C}_{nn}F_s\left(\mathbf{D}_{nx}N_j\right)\right] \\ & + \left(\mathbf{D}_p F_\tau\right)^T N_i \left[\mathbf{C}_{pp}\left(\mathbf{D}_p F_s\right) N_j + \mathbf{C}_{pn}\left(\mathbf{D}_{np}F_s\right) N_j + \mathbf{C}_{pn}F_s\left(\mathbf{D}_{nx}N_j\right)\right] \Big\} \, d\Omega \; dx \; \mathbf{q}_{sj} \\ & - \delta\mathbf{q}_{\tau i}^T \int_{l_e}\int_{\Omega} \left[\mathbf{D}_p^T F_\tau N_i \boldsymbol{\lambda}_{\mathbf{p}} + \left(\mathbf{D}_{nx}^T + \mathbf{D}_{np}^T\right) F_\tau N_i \boldsymbol{\lambda}_{\mathbf{n}}\right] \Theta_\Omega \Theta_n \; d\Omega \; dx\end{aligned}$$

This latter can be written in a compact vector form:

$$\delta L_{\text{int}} = \delta\mathbf{q}_{\tau i}^T \mathbf{K}_{uu}^{\tau sij} \mathbf{q}_{sj} - \delta\mathbf{q}_{\tau i}^T \mathbf{K}_{u\theta}^{\tau i}. \tag{21}$$

The components of the stiffness matrix fundamental nucleus $\mathbf{K}_{uu}^{\tau sij} \in \mathbb{R}^{3\times 3}$ are:

$$\begin{aligned}
K_{uuxx}^{\tau sij} &= I_{i,_x j,_x} J_{\tau s}^{11} + I_{i,_x j} J_{\tau s,_y}^{16} + I_{ij,_x} J_{\tau,_y s}^{16} + I_{ij}\left(J_{\tau,_z s,_z}^{55} + J_{\tau,_y s,_y}^{66}\right) \\
K_{uuxy}^{\tau sij} &= I_{ij,_x} J_{\tau,_y s}^{12} + I_{i,_x j,_x} J_{\tau s}^{16} + I_{ij}\left(J_{\tau,_y s,_y}^{26} + J_{\tau,_z s,_x}^{45}\right) + I_{i,_x j} J_{\tau s,_y}^{66} \\
K_{uuxz}^{\tau sij} &= I_{ij,_x} J_{\tau,_z s}^{13} + I_{ij}\left(J_{\tau,_z s,_y}^{36} + J_{\tau,_y s,_z}^{45}\right) + I_{i,_x j} J_{\tau s,_z}^{55} \\
K_{uuyx}^{\tau sij} &= I_{i,_x j} J_{\tau s,_y}^{12} + I_{i,_x j,_x} J_{\tau s}^{16} + I_{ij}\left(J_{\tau,_y s,_y}^{26} + J_{\tau,_z s,_z}^{45}\right) + I_{ij,_x} J_{\tau,_y s}^{66} \\
K_{uuyy}^{\tau sij} &= I_{ij}\left(J_{\tau,_y s,_y}^{22} + J_{\tau,_z s,_z}^{44}\right) + I_{ij,_x} J_{\tau,_y s}^{26} + I_{i,_x j} J_{\tau s,_y}^{26} + I_{i,_x j,_x} J_{\tau s}^{66} \\
K_{uuyz}^{\tau sij} &= I_{ij}\left(J_{\tau,_z s,_y}^{23} + J_{\tau,_y s,_z}^{44}\right) + I_{ij,_x} J_{\tau,_z s}^{36} + I_{i,_x j} J_{\tau s,_z}^{45} \\
K_{uuzx}^{\tau sij} &= I_{i,_x j} J_{\tau s,_z}^{13} + I_{ij}\left(J_{\tau,_y s,_z}^{36} + J_{\tau,_z s,_y}^{45}\right) + I_{ij,_x} J_{\tau,_z s}^{55} \\
K_{uuzy}^{\tau sij} &= I_{ij}\left(J_{\tau,_y s,_z}^{23} + J_{\tau,_z s,_y}^{44}\right) + I_{i,_x j} J_{\tau s,_z}^{36} + I_{ij,_x} J_{\tau,_z s}^{45} \\
K_{uuzz}^{\tau sij} &= I_{ij}\left(J_{\tau,_z s,_z}^{33} + J_{\tau,_y s,_y}^{44}\right) + I_{ij,_x} J_{\tau,_y s}^{45} + I_{i,_x j} J_{\tau s,_y}^{45} + I_{i,_x j,_x} J_{\tau s}^{55}
\end{aligned} \tag{22}$$

$J_{\tau_{(,\phi)}s_{(,\xi)}}^{gh}$ is a cross-section moment:

$$J_{\tau_{(,\phi)}s_{(,\xi)}}^{gh} = \int_{\Omega} C_{gh} F_{\tau_{(,\phi)}} F_{s_{(,\xi)}} \; d\Omega \tag{23}$$

It is computed as a weighted sum (in the continuum) of each elemental cross-section area where the weight functions account for the spatial distribution of the geometry and the material. $I_{i_{(,x)}j_{(,x)}}$ is:

$$I_{i_{(,x)}j_{(,x)}} = \int_{l_e} N_{i_{(,x)}} N_{j_{(,x)}} \; dx \tag{24}$$

Subscript 'x', when preceded by comma, represents derivation versus the x-coordinate. Integrals I are numerically evaluated through Gauss' quadrature method. Shear locking is corrected through a selective integration technique. Two, three and four quadrature points are used for full integration for B2, B3 and B4 elements, respectively. One point less is used for the selective integration. The selected under-integrated term is I_{ij} in $K_{uuxx}^{\tau sij}$ that is related to shear deformations γ_{xy} and γ_{xz}.

The components of the thermo-mechanical coupling vector $\mathbf{K}_{u\theta}^{\tau i} \in \mathbb{R}^3$ are:

$$\begin{aligned}
K_{u\theta x}^{\tau i} &= I_{\theta_n i,_x} J_{\theta_\Omega \tau}^{1} + I_{\theta_n i} J_{\theta_\Omega \tau,_y}^{6} \\
K_{u\theta y}^{\tau i} &= I_{\theta_n i} J_{\theta_\Omega \tau,_y}^{2} + I_{\theta_n i,_x} J_{\theta_\Omega \tau}^{6} \\
K_{u\theta z}^{\tau i} &= I_{\theta_n i} J_{\theta_\Omega \tau,_z}^{3}
\end{aligned} \tag{25}$$

The generic term $J^{g}_{\theta_\Omega \tau_{(,\phi)}}$ stands for:

$$J^{g}_{\theta_\Omega \tau_{(,\phi)}} = \int_{\Omega} F_{\tau_{(,\phi)}} \ \lambda_g \ \Theta_\Omega \left(y, z\right) \ d\Omega. \tag{26}$$

whereas $I_{\theta_n j_{(,x)}}$ is:

$$I_{\theta_n i_{(,x)}} = \int_{l_e} N_{i_{(,x)}} \Theta_n \left(x\right) \ dx. \tag{27}$$

A classical one-way staggered solution method is used (see Nowiski [28]). The temperature field deriving by a Navier-type closed form solution of Fourier's equation is integrated over the cross-section and along the axis in order to obtain a thermal load variationally consistent with the proposed models. Five Gauss' quadrature points are used in order to correctly compute the integral in Eq. 27. Once the displacement approximation order N and the number of nodes per element N^e_n have been fixed, the element stiffness matrix is straightforwardly obtained by assembling the fundamental nuclei of Eqs. 22 coming from each term of the displacement expansion in Eq. 16.

5 Numerical Results and Discussion

The beam support is $[0, l] \times [0, a] \times [0, b]$ with l the length, b the thickness and a the width (see Fig. 1). The cross-section is square with $a = b = 1$ m. Slender beams ($l/b = 100$) and short beams ($l/b = 5$) are investigated. Simply supported and cantilever beams made of a functionally graded ceramic-metal material are considered. A ceramic phase made of Zirconia (ZrO_2) and a metallic phase of Monel (70Ni-30Cu), a nikel-based alloy, are assumed. Materials properties are presented in Table. 2. A power law is assumed for the variation of the generic material property, f, along the thickness coordinate z:

$$f = \left(f_1 - f_2\right) \left(\alpha_z z + \beta_z\right)^{n_z} + f_2 \tag{28}$$

This law is derived from the rule of mixtures, assuming a power gradation law of the volume fraction of the two constituent materials, see Reddy [29] and Chakraborty et al. [3]. f_i is the generic material property of each constituent, n_z is the power law exponent and, for the assumed reference system, $\alpha_z = 1/b$ and $\beta_z = 0$. Different values of n_z are considered in the following analyses. The boundary conditions for the over-temperature at beam top ($z/b = 1$) and bottom ($z/b = 0$) surfaces are: $T_t = 150$ K and $T_b = 50$ K. As far as the temperature variation along the beam axis, the half-wave number m is equal to one, see Appendix. Results provided by the proposed family of one-dimensional finite elements are compared with three-dimensional finite elements solutions obtained via the commercial software ANSYS. For the latter analysis, tri-quadratic 20-node element "Solid90" and "Solid186" are used for the thermal and mechanical problem, respectively.
For the FGM characterisation, each element is considered as homogeneous with the material properties corresponding to the values at its central point. The accuracy of the three-dimensional FEM solution is influenced by both the FEM approximation and the approximation of the material gradation law. Two different meshes are considered for the three-dimensional finite element solution for each analysis. In the case of short beams, the acronym FEM 3D-R stands for a refined model with a $60 \times 60 \times 60$ elements mesh, whereas the coarse $20 \times 20 \times 20$ mesh solution is addressed by FEM 3D-C. In the case of slender beams, FEM 3D-R refers to a refined model with a $160 \times 32 \times 32$ elements mesh, and FEM 3D-C stands for a coarser $100 \times 20 \times 20$ mesh.

About the computational costs, the number of degrees of freedom (N_{DOFs}) of the present one-dimensional finite elements is related to the expansion order N and the total number of nodes N_n through the equation:

$$N_{DOFs} = 3 \cdot \frac{(N+1)(N+2)}{2} \cdot N_n \tag{29}$$

In the case of the most refined one-dimensional model used in the analysis (a 13th-order approximation and 121 nodes), N_{DOFs} is about $3.8 \cdot 10^4$. A very refined mesh ($60 \times 60 \times 60$ elements) is required for three-dimensional model in order to accurately predict the stress state induced by the thermal load. N_{DOFs} for this mesh is equal to about $2.7 \cdot 10^6$. N_{DOFs} for the coarse mesh ($20 \times 20 \times 20$ elements) is about $1.1 \cdot 10^5$.

5.1 Simply supported beams

Simply supported beams are first investigated. The temperature variation along the thickness at the mid-span section in presented in Fig. 4 for different values of l/b. The temperature profile has been obtained via the procedure presented in the Appendix. Fourier's heat conduction equation was analytically solved for a FGM beam by considering 16 fictitious layers. A good agreement between the closed-form solution and FEM 3D-R solution is found. The strain energy error versus the dimensionless distance between two consecutive nodes δ_{ii+1}/l is evaluated for linear, quadratic and cubic elements:

$$\Delta_E = \frac{L_{\text{int}}^{\text{Nav}} - L_{\text{int}}^{\text{FEM}}}{L_{\text{int}}^{\text{Nav}}} \tag{30}$$

Results provided by finite elements are assessed towards an exact Navier-type analytical solution within the framework of the present formulation. The presented results have been obtained for $N = 2$ and $l/b = 5$. Nevertheless, solutions for different expansion orders N, length-to-side ratios and FGM gradation law exponent n_z are very similar. As a good compromise between accuracy of results and computational costs, a number of nodes N_n equal to 121 (corresponding to $\delta_{ii+1}/l = 0.008\overline{3}$) is assumed for all the following analyses.
In order to avoid the shear-locking phenomenon affecting linear elements, a selective integration was adopted. Fig. 3 shows the comparison between selective and full integration strategies. The variation of $\hat{u}_z$:

$$\hat{u}_z = \frac{u_z^{\text{FEM}}}{u_z^{\text{Nav}}} \tag{31}$$

computed at $(x/l, y/a, z/b) = (1/2, 0, 0)$ via B2 elements versus l/b is presented. It can be clearly seen that a selective integration is free of locking and that it is effective regardless the beam theory order N.
As far as the following tables are concerned, displacements and stresses are evaluated at the following points:

$$\begin{array}{ccc} \overline{u}_x = u_x\,(0, a/2, b) & \overline{u}_y = u_y\,(l/2, a, b) & \overline{u}_z = u_z\,(l/2, a/2, b/2) \\ \overline{\sigma}_{xx} = \sigma_{xx}\,(l/2, a/2, b/2) & \overline{\sigma}_{xy} = \sigma_{zz}\,(0, a/4, 0) & \overline{\sigma}_{xz} = \sigma_{xz}\,(0, 0, b/2) \\ \overline{\sigma}_{yy} = \sigma_{yy}\,(l/2, a/2, b/2) & \overline{\sigma}_{zz} = \sigma_{zz}\,(l/2, a/2, b/2) & \overline{\sigma}_{yz} = \sigma_{yz}\,(l/2, a/4, 3/4b) \end{array} \tag{32}$$

Table 3 shows the displacement components for a slender beam in the case of $n_z = 1$. The relative difference between the results provided by theories with order $N > 7$ and the three-dimensional reference solution is 1.1%, at worst. Results computed via Timoshenko's (TBT) as well as Euler-Bernoulli's (EBT) classical models are also presented in order to show that higher order models should be used to accurately predict all the three displacement components. TBT and EBT results have been obtained using a Navier-type closed form solution valid for simply supported boundary conditions. The displacements for a very short beam with $n_z = 1$ are presented in Table 4. The relative difference between results provided by a theory with N as low as 4 and

the reference solution is lower than 1.6%. Tables 5 and 6 show the stress components for a very short beam. Higher-order theories are in good agreement with the three-dimensional finite element solution. In the case of a 13th-order theory and cubic elements, the error is 3.3%, at worst.

5.2 Cantilever beams

In the case of cantilever beams, the following displacements and stresses are considered:

$$\begin{array}{ccc} \overline{u}_x = u_x\left(l, a/2, b\right) & \overline{u}_y = u_y\left(l/2, a, b\right) & \overline{u}_z = u_z\left(l, a/2, b/2\right) \\ \overline{\sigma}_{xx} = \sigma_{xx}\left(l/2, a/2, b/4\right) & \overline{\sigma}_{xy} = \sigma_{zz}\left(l/4, a/4, b\right) & \overline{\sigma}_{xz} = \sigma_{xz}\left(l/4, a/2, b/2\right) \\ \overline{\sigma}_{yy} = \sigma_{yy}\left(l/2, a/2, b/2\right) & \overline{\sigma}_{zz} = \sigma_{zz}\left(l/2, a/2, b/2\right) & \overline{\sigma}_{yz} = \sigma_{yz}\left(l/2, a/4, 3/4b\right) \end{array} \tag{33}$$

Displacement components for a slender beam with $n_z = 1$ are presented in Table 7. The relative difference on the primary displacements u_z and u_x between the results provided by one-dimensional finite elements with N as low as 3 and the three-dimensional reference solution is 1.1%, at worst. The error on the secondary displacement u_y is about 7%. Table 8 shows the displacements for a very short beam with $n_z = 1$. The error for theories with N as low as 4 is about 1.6%. Tables 9 and 10 present the stress values for a very short beam. It should be noticed that stresses evaluated at the mid-span section are not influenced by the boundary conditions at the ends of the beam since they are very close to those for the simply supported case. Higher-order one-dimensional finite elements lead to results that are very close to the reference solution. In the case of a 13th-order theory and cubic elements, the error is 3.3% at worst. In Figs. 5 to 12, the variation of displacements and stresses evaluated in the most representative cross-sections of a short beam in the form of a colour map for $n_z = 0.5$, $n_z = 1$ and $n_z = 2$. Figs. 5 and 6 present the variation of displacements u_x and u_y over the cross-section. Transverse displacement u_z reaches its maximum value at the free section, where it is constant. The corresponding cross-section figure is not shown for the sake of brevity. Stress components are presented in Figs. 7 to 12. They are are evaluated at an opportune distance from the clamped end where, as it is well known, stress singularities are present. Results show that higher-order one-dimensional theories like $N = 13$ are able to fairly predict both displacements and stresses for different material gradation laws. Some major difficulties can be noticed regarding the prediction of σ_{zz} for $n_z = 0.5$. In order to further improve the accuracy of the results in future works, the adoption of a layerwise approach in stead of an equivalent-single-layer theory could be recommended.

6 Conclusions

A family of one-dimensional finite elements derived through a Unified Formulation was proposed for the thermoelastic analysis of three-dimensional functionally graded beam structures. The temperature profile was obtained via a Navier-type solution of Fourier's heat conduction equation. Simply supported and cantilever beams were investigated, for different length-to-side ratios and different material gradation profiles. Results were assessed towards three-dimensional FEM solutions obtained via the commercial code ANSYS. Beams under thermal stresses present a complex three-dimensional stress state that calls for very accurate models. Results of the investigations demonstrated that UF-derived one-dimensional finite elements are a convenient choice for an accurate yet computationally efficient thermal stress analysis of FGM beams.

Acknowledgements

This work has been partially supported by the European Union within the Horizon 2020 research and innovation programme under grant agreement No 642121.

References

[1] R. B. Hetnarski and M. R. Eslami. *Thermal stresses - Advanced theory and applications*. Springer, 2009.

[2] N. Noda. Thermal stresses in functionally graded materials. *Journal of Thermal Stresses*, 22(4-5):477–512, 1999.

[3] A. Chakraborty, S. Gopalakrishnan, and J. N. Reddy. A new beam finite element for the analysis of functionally graded materials. *International Journal of Mechanical Sciences*, 45(3):519–539, 2003.

[4] A. Carpinteri and M. Paggi. Thermo-elastic mismatch in nonhomogeneous beams. *Journal of Engineering Mathematics*, 61(2-4):371–384, 2008.

[5] H. Wang and Q.-H. Qin. Meshless approach for thermo-mechanical analysis of functionally graded materials. *Engineering Analysis with Boundary Elements*, 32(9):704–712, 2008.

[6] A. Mahi, E. A. Adda Bedia, A. Tounsi, and I. Mechab. An analytical method for temperature-dependent free vibration analysis of functionally graded beams with general boundary conditions. *Composite Structures*, 92(8):1877–1887, 2010.

[7] N. Wattanasakulpong, B. Gangadhara Prusty, and Kelly D.W. Thermal buckling and elastic vibration of third-order shear deformable functionally graded beams. *International Journal of Mechanical Sciences*, 53(9):734–743, 2011.

[8] Y. S. Touloukian. *Thermophysical properties of high temperature solid materials*. MacMillan, New York, 1967.

[9] H.J. Xiang and J. Yang. Free and forced vibration of a laminated FGM Timoshenko beam of variable thickness under heat conduction. *Composites Part B: Engineering*, 39(2):292–303, 2008.

[10] B.V. Sankar and J.T. Tzeng. Thermal stresses in functionally graded beams. *AIAA Journal*, 40(6):1228–1232, 2002.

[11] B. V. Sankar. An elasticity solution for functionally graded beams. *Composites Science and Technology*, 61(5):689–696, 2001.

[12] M. Lezgy-Nazargah. Fully coupled thermo-mechanical analysis of bi-directional FGM beams using NURBS isogeometric finite element approach. *Aerospace Science and Technology*, 45:154–164, 2015.

[13] Y. Kiani and M.R. Eslami. Thermal buckling analysis of functionally graded material beams. *International Journal of Mechanics and Materials in Design*, 6(3):229–238, 2010.

[14] D.G. Zhang. Nonlinear bending analysis of FGM beams based on physical neutral surface and high order shear deformation theory. *Composite Structures*, 100:121–126, 2013.

[15] T. Kocaturk and S.D. Akbas. Post-buckling analysis of Timoshenko beams made of functionally graded material under thermal loading. *Structural Engineering and Mechanics*, 41(6):775–789, 2012.

[16] Y. Sun, S.R. Li, and R.C. Batra. Thermal buckling and post-buckling of FGM Timoshenko beams on nonlinear elastic foundation. *Journal of Thermal Stresses*, 39(1):11–26, 2016.

[17] E. Carrera. Theories and finite elements for multilayered plates and shells: a unified compact formulation with numerical assessment and benchmarking. *Archives of Computational Methods in Engineering*, 10(3):215–296, 2003.

[18] E. Carrera, G. Giunta, and M. Petrolo. *Beam Structures: Classical and Advanced Theories*. John Wiley and Sons, 2011.

[19] G. Giunta, S. Belouettar, and E. Carrera. Analysis of FGM beams by means of classical and advanced theories. *Mechanics of Advanced Materials and Structures*, 17(8):622–635, 2010.

[20] G. Giunta, D. Crisafulli, S. Belouettar, and E. Carrera. Hierarchical theories for the free vibration analysis of functionally graded beams. *Composite Structures*, 94(1):68–74, 2011.

[21] G. Giunta, Y. Koutsawa, S. Belouettar, and H. Hu. Static, free vibration and stability analysis of three-dimensional nano-beams by atomistic refined models accounting for surface free energy effect. *International Journal of Solids and Structures*, 50(9):1460–1472, 2013.

[22] G. Giunta, N. Metla, Y. Koutsawa, and S. Belouettar. Free vibration and stability analysis of three-dimensional sandwich beams via hierarchical models. *Composites Part B: Engineering*, 47:326–338, 2013.

[23] A. Catapano, G. Giunta, S. Belouettar, and E. Carrera. Static analysis of laminated beams via a unified formulation. *Composite Structures*, 94(1):75–83, 2011.

[24] G. Giunta, D. Crisafulli, S. Belouettar, and E. Carrera. A thermo-mechanical analysis of functionally graded beams via hierarchical modelling. *Composite Structures*, 95:676–690, 2013.

[25] G. Giunta, N. Metla, S. Belouettar, A. J. M. Ferreira, and E. Carrera. A thermo-mechanical analysis of isotropic and composite beams via collocation with radial basis functions. *Journal of Thermal Stresses*, 36(11):1169–1199, 2013.

[26] G. Giunta, G. De Pietro, H. Nasser, S. Belouettar, E. Carrera, and M. Petrolo. A thermal stress finite element analysis of beam structures by hierarchical modelling. *Composites Part B: Engineering*, 95:179–195, 2016.

[27] G. M. Philips. *Interpolation and approximation by polynomials*. Springer-Verlag, 2003.

[28] J. L. Nowinski. *Theory of thermoelasticity with applications*. Sijthoff and Noordhoff, The Netherlands, 1978.

[29] G. N. Praveen and J. N. Reddy. Nonlinear transient thermoelastic analysis of functionally graded ceramic-metal plates. *International Journal of Solids and Structures*, 35(33):4457–4476, 1998.

Appendix

The temperature is as an external load within the mechanical analysis, as it is shown in Section 4. The temperature profile over the beam domain is obtained by analytically solving Fourier's heat conduction equation for FGM beams. The cross-section Ω is divided into N_Ω^k non-overlapping sub-domains along the through-the-thickness direction z:

$$\Omega = \bigcup_{k=1}^{N_{\Omega^k}} \Omega^k \tag{34}$$

Each sub-domain is considered to be homogeneous, being the generic material property equal to the value at sub-domain's centre. Fourier differential equation for a k^{th} homogeneous sub-domain reads:

$$\frac{\partial^2 T^k}{\partial x^2} + \frac{\partial^2 T^k}{\partial y^2} + \frac{\partial^2 T^k}{\partial z^2} = 0 \tag{35}$$

In order to analytically solve this latter equation, a constant temperature along the through-the-width coordinate y is assumed. This also leads to no material gradation along the through-the-width coordinate. At the interfaces between two adjacent sub-domains, the continuity of the temperature and the through-the-thickness heat flux q_z is imposed :

$$\begin{aligned} T_t^k &= T_b^{k+1} \\ q_{zt}^k &= q_{zb}^{k+1} \end{aligned} \tag{36}$$

Subscripts 't' and 'b' stand for sub-domain's top and bottom, respectively. The through-the-thickness heat flux is given by:

$$q_z^k = K^k \frac{\partial T^k}{\partial z} \tag{37}$$

where K^k is the thermal conductivity. Over-temperature boundary conditions are imposed at through-the-thickness top and bottom of the beam as:

$$\begin{aligned} T &= T_t \sin(\alpha x) \\ T &= T_b \sin(\alpha x) \end{aligned} \tag{38}$$

T_t and T_b are the maximal amplitudes and α is:

$$\alpha = \frac{m\pi}{l}, \tag{39}$$

with $m \in \mathbf{N}^+$ being the half-wave number along the beam axis. The following temperature profile:

$$T^k(x,z) = \Theta_\Omega^k(z) \sin(\alpha x) = T_0^k \exp(sz) \sin(\alpha x) \tag{40}$$

represents a solution of the considered heat conduction problem. T_0^k is an unknown constant obtained by imposing the boundary condition, whereas the term s is obtained by replacing Eq. 40 into Eq. 35:

$$s_{1,2} = \pm\alpha \tag{41}$$

$\Theta_\Omega^k(z)$, therefore, becomes:

$$\Theta_\Omega^k(z) = T_{01}^k \exp(+\alpha z) + T_{02}^k \exp(-\alpha z) \tag{42}$$

or, equivalently:

$$\Theta_\Omega^k(z) = C_1^k \cosh(\alpha z) + C_2^k \sinh(\alpha z) \tag{43}$$

where C_i^k are a set of $2 \cdot N_{\Omega^k}$ unknowns to be obtained form the $2(N_{\Omega^k} - 1)$ interface conditions in Eqs. 36 and the two boundary conditions at beam top and bottom, see Eq. 38. A solution convergence versus N_{Ω^k} has been investigated, but it is not reported for the sake of brevity. $N_{\Omega^k} = 16$ is shown to ensure a converged temperature profile for the considered FGM.

Tables

N	N_u	F_τ
0	1	$F_1 = 1$
1	3	$F_2 = y \quad F_3 = z$
2	6	$F_4 = y^2 \quad F_5 = yz \quad F_6 = z^2$
3	10	$F_7 = y^3 \quad F_8 = y^2 z \quad F_9 = yz^2 \quad F_{10} = z^3$
...	...	...
N	$\frac{(N+1)(N+2)}{2}$	$F_{\frac{(N^2+N+2)}{2}} = y^N \quad F_{\frac{(N^2+N+4)}{2}} = y^{N-1}z \quad \dots \quad F_{\frac{N(N+3)}{2}} = yz^{N-1} \quad F_{\frac{(N+1)(N+2)}{2}} = z^N$

Table 1: Mac Laurin's polynomials terms via Pascal's triangle.

	E [GPa]	ν	K [W/mK]	α [10^{-6} K^{-1}]
Zirconia	151.01	0.300	2.09	10.
Monel	179.40	0.368	25.00	15.

Table 2: FGM constituents elastic and thermal properties.

	$10 \times \overline{u}_z$		$-10^2 \times \overline{u}_x$		$10^4 \times \overline{u}_y$		
FEM 3D-R[a]	6.0649		4.0744		7.1355		
FEM 3D-C[b]	6.1071		4.0855		7.0892		
TBT[c]	6.1451		4.0954		0.0000		
EBT[c]	6.1455		4.0953		0.0000		
	B2	B3, B4	B2	B3, B4	B2	B3	B4
$N = 13$	6.1325	6.1328	4.0932	4.0933	7.1132	7.1123	7.1126
$N = 11$	6.1325	6.1328	4.0932	4.0933	7.1102	7.1094	7.1097
$N = 8$	6.1325	6.1328	4.0932	4.0933	7.1010	7.1001	7.1004
$N = 5$	6.1319	6.1322	4.0931	4.0932	7.0047	7.0039	7.0042
$N = 2$	5.9689	5.9692	4.0669	4.0669	6.3885	6.3877	6.3880

a: Elements' number $160 \times 32 \times 32$. *b*: Elements' number $100 \times 20 \times 20$.
c: Navier-type solution.

Table 3: Displacement components $\overline{u}_z$, $\overline{u}_x$ and $\overline{u}_y$ [m] for a slender FGM simply supported beam, $n_z = 1$.

	$10^3 \times \overline{u}_z$		-$10^3 \times \overline{u}_x$		$10^4 \times \overline{u}_y$		
FEM 3D-R[a]	1.4917		1.9976		6.9765		
FEM 3D-C[b]	1.5089		2.0064		7.0247		
TBT[c]	1.4956		1.9809		0.0000		
EBT[c]	1.4957		1.9808		0.0000		
	B2	B3, B4	B2	B3, B4	B2	B3	B4
$N = 13$	1.5160	1.5161	2.0107	2.0107	7.0261	7.0255	7.0256
$N = 10$	1.5160	1.5161	2.0106	2.0107	7.0203	7.0197	7.0197
$N = 7$	1.5160	1.5161	2.0111	2.0112	6.9947	6.9942	6.9942
$N = 4$	1.5158	1.5159	2.0066	2.0066	6.8768	6.8763	6.8763
$N = 2$	1.4553	1.4554	2.0030	2.0030	6.1463	6.1458	6.1458

a: Elements' number $60 \times 60 \times 60$. *b*: Elements' number $20 \times 20 \times 20$.
c: Navier-type solution.

Table 4: Displacement components $\overline{u}_z$, $\overline{u}_x$ and $\overline{u}_y$ [m] for a short FGM simply supported beam, $n_z = 1$.

	$10^{-6} \times \overline{\sigma}_{xx}$			$10^{-5} \times \overline{\sigma}_{xy}$			-$10^{-6} \times \overline{\sigma}_{xz}$		
FEM 3D-R[a]	8.5121			9.6899			2.9668		
FEM 3D-C[b]	8.7013			9.8166			2.9902		
TBT[c]	10.245			0.0000			0.0000		
EBT[c]	10.233			_[d]			_[d]		
	B2	B3	B4	B2	B3	B4	B2	B3	B4
$N = 13$	8.7748	8.8411	8.7890	9.8564	9.8253	9.8426	3.0193	2.9964	3.0093
$N = 11$	8.8734	8.9397	8.8876	9.7936	9.7625	9.7798	3.0138	2.9909	3.0038
$N = 9$	8.8863	8.9524	8.9005	9.8572	9.8262	9.8435	2.9891	2.9663	2.9791
$N = 7$	8.8519	8.9186	8.8662	10.057	10.026	10.043	3.0873	3.0645	3.0773
$N = 4$	6.3049	6.3717	6.3193	1.8705	1.8403	1.8576	2.8007	2.7779	2.7907
$N = 2$	22.250	22.316	22.264	25.875	25.844	25.860	2.8220	2.8002	2.8125

a: Elements' number $60 \times 60 \times 60$. *b*: Elements' number $20 \times 20 \times 20$.
c: Navier-type solution. *d*: Result not provided by the theory.

Table 5: Stress components $\overline{\sigma}_{xx}$, $\overline{\sigma}_{xy}$ and $\overline{\sigma}_{xz}$ [Pa] for a short FGM simply supported beam, $n_z = 1$.

	$10^{-6} \times \overline{\sigma}_{yy}$			$10^{-6} \times \overline{\sigma}_{zz}$			-$10^{-6} \times \overline{\sigma}_{yz}$	
FEM 3D-R[a]	4.7891			6.3622			4.0031	
FEM 3D-C[b]	4.8664			6.4933			4.1017	
	B2	B3	B4	B2	B3	B4	B2	B3, B4
$N = 13$	4.9353	4.9490	4.9229	6.4851	6.4987	6.4726	4.0826	4.0824
$N = 11$	5.0380	5.0518	5.0256	6.6771	6.6909	6.6646	4.0817	4.0815
$N = 9$	5.0549	5.0684	5.0426	6.6987	6.7121	6.6863	4.0294	4.0292
$N = 7$	4.9814	4.9957	4.9690	6.6642	6.6784	6.6518	3.9214	3.9212
$N = 4$	1.9721	1.9866	1.9599	1.9702	1.9846	1.9580	1.7367	1.7366
$N = 2$	26.398	26.411	26.385	26.845	26.857	26.832	0.0552	0.0552

a: Elements' number $60 \times 60 \times 60$. *b*: Elements' number $20 \times 20 \times 20$.
c: Navier-type solution.

Table 6: Stress components $\overline{\sigma}_{yy}$, $\overline{\sigma}_{zz}$ and $\overline{\sigma}_{yz}$ [Pa] for a short FGM simply supported beam, $n_z = 1$.

	$-\overline{u}_z$	$10^2 \times \overline{u}_x$		$10^4 \times \overline{u}_y$		
FEM 3D-R[a]	1.9053	8.1478		6.6560		
FEM 3D-C[b]	1.9185	8.1689		7.0411		
	B2,B3,B4	B2	B3, B4	B2	B3	B4
$N = 13$	1.9266	8.1865	8.1865	7.1132	7.1123	7.1126
$N = 9$	1.9266	8.1865	8.1865	7.1067	7.1058	7.1061
$N = 6$	1.9264	8.1863	8.1863	7.0472	7.0464	7.0467
$N = 3$	1.9254	8.1852	8.1853	6.8717	6.8709	6.8712
$N = 2$	1.8752	8.1337	8.1337	6.3885	6.3877	6.3880

a: Elements' number $60 \times 60 \times 60$. *b*: Elements' number $20 \times 20 \times 20$.

Table 7: Displacement components $\overline{u}_z$, $\overline{u}_x$ and $\overline{u}_y$ [m] for a slender FGM cantilever beam, $n_z = 1$.

	$-10^3 \times \overline{u}_z$			$10^3 \times \overline{u}_x$			$10^4 \times \overline{u}_y$		
FEM 3D-R[a]		4.6144			3.9723			6.9765	
FEM 3D-C[b]		4.6669			3.9899			7.0240	
	B2	B3	B4	B2	B3	B4	B2	B3	B4
$N = 13$	4.6893	4.6895	4.6896	3.9986	3.9985	3.9984	7.0261	7.0255	7.0256
$N = 11$	4.6893	4.6895	4.6896	3.9986	3.9984	3.9984	7.0229	7.0223	7.0224
$N = 8$	4.6894	4.6896	4.6897	3.9988	3.9986	3.9986	7.0124	7.0119	7.0119
$N = 4$	4.6867	4.6868	4.6869	3.9953	3.9952	3.9952	6.8768	6.8763	6.8763
$N = 2$	4.5242	4.5243	4.5243	3.9814	3.9814	3.9814	6.1463	6.1458	6.1458

a: Elements' number $60 \times 60 \times 60$. *b*: Elements' number $20 \times 20 \times 20$.

Table 8: Displacement components $\overline{u}_z$, $\overline{u}_x$ and $\overline{u}_y$ [m] for a short FGM cantilever beam, $n_z = 1$.

	$10^{-6} \times \overline{\sigma}_{xx}$			-$10^{-6} \times \overline{\sigma}_{xy}$			$10^{-6} \times \overline{\sigma}_{xz}$		
FEM 3D-R[a]		8.5121			2.3812			1.4490	
FEM 3D-C[b]		8.7014			2.4166			1.4815	
	B2	B3	B4	B2	B3	B4	B2	B3	B4
$N = 13$	8.7749	8.8410	8.7890	2.2846	2.4063	2.4050	0.9233	1.4857	1.4767
$N = 11$	8.8734	8.9397	8.8875	2.3079	2.4295	2.4282	0.9185	1.4810	1.4719
$N = 9$	8.8864	8.9524	8.9005	2.3342	2.4558	2.4545	0.9242	1.4867	1.4775
$N = 7$	8.8520	8.9185	8.8661	2.4193	2.5414	2.5398	0.9178	1.4803	1.4712
$N = 4$	6.3049	6.3715	6.3191	1.2997	1.4227	1.4217	0.7969	1.3593	1.3502
$N = 2$	22.250	22.315	22.264	1.9555	2.0653	2.0634	-0.5945	-0.0544	-0.0632

a: Elements' number $60 \times 60 \times 60$. *b*: Elements' number $20 \times 20 \times 20$.

Table 9: Stress components $\overline{\sigma}_{xx}$, $\overline{\sigma}_{xy}$ and $\overline{\sigma}_{xz}$ [Pa] for a short FGM cantilever beam, $n_z = 1$.

	$10^{-6} \times \overline{\sigma}_{yy}$			$10^{-6} \times \overline{\sigma}_{zz}$			-$10^{-6} \times \overline{\sigma}_{yz}$		
FEM 3D-R[a]		4.7895			6.3625			4.0032	
FEM 3D-C[b]		4.8667			6.4935			4.1018	
	B2	B3	B4	B2	B3	B4	B2	B3	B4
$N = 13$	4.9357	4.9494	4.9233	6.4854	6.4990	6.4729	4.0826	4.0824	4.0824
$N = 11$	5.0384	5.0522	5.0260	6.6774	6.6911	6.6649	4.0817	4.0815	4.0815
$N = 9$	5.0554	5.0688	5.0430	6.6990	6.7124	6.6865	4.0295	4.0293	4.0293
$N = 7$	4.9819	4.9961	4.9695	6.6645	6.6787	6.6521	3.9214	3.9212	3.9212
$N = 4$	1.9724	1.9868	1.9602	1.9703	1.9847	1.9581	1.7367	1.7366	1.7366
$N = 2$	26.398	26.411	26.385	26.845	26.857	26.832	0.0552	0.0552	0.0055

a: Elements' number $60 \times 60 \times 60$. *b*: Elements' number $20 \times 20 \times 20$.

Table 10: Stress components $\overline{\sigma}_{yy}$, $\overline{\sigma}_{zz}$ and $\overline{\sigma}_{yz}$ [Pa] for a short FGM cantilever beam, $n_z = 1$.

Figures

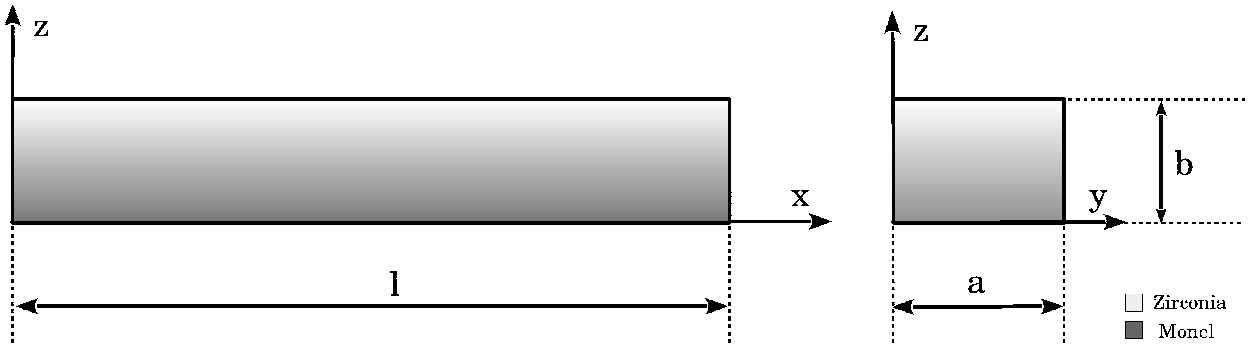

Figure 1: FGM beam geometry and reference system.

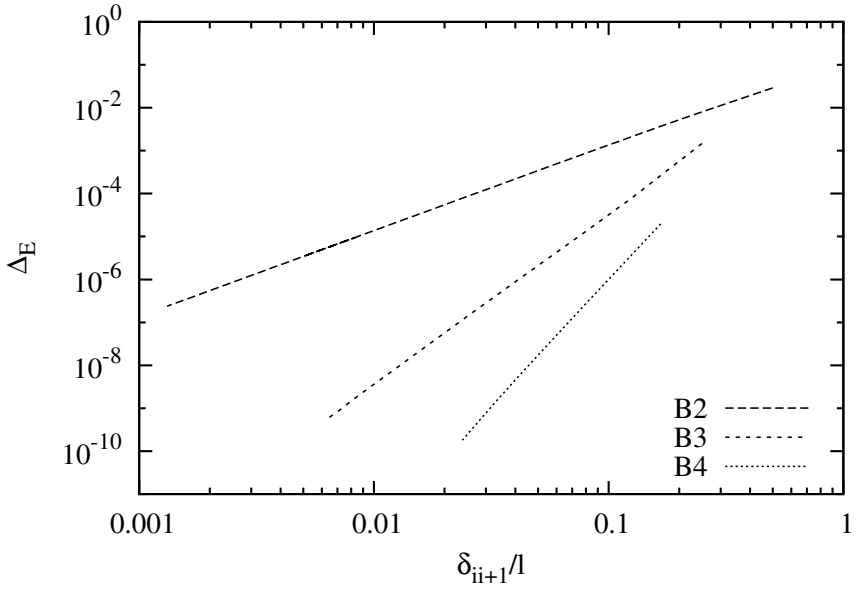

Figure 2: Relative strain energy error (with reference to Navier closed form solution) versus the dimensionless distance between two consecutive nodes, short simply supported FGM beam, $n_z = 1$ and $N = 2$.

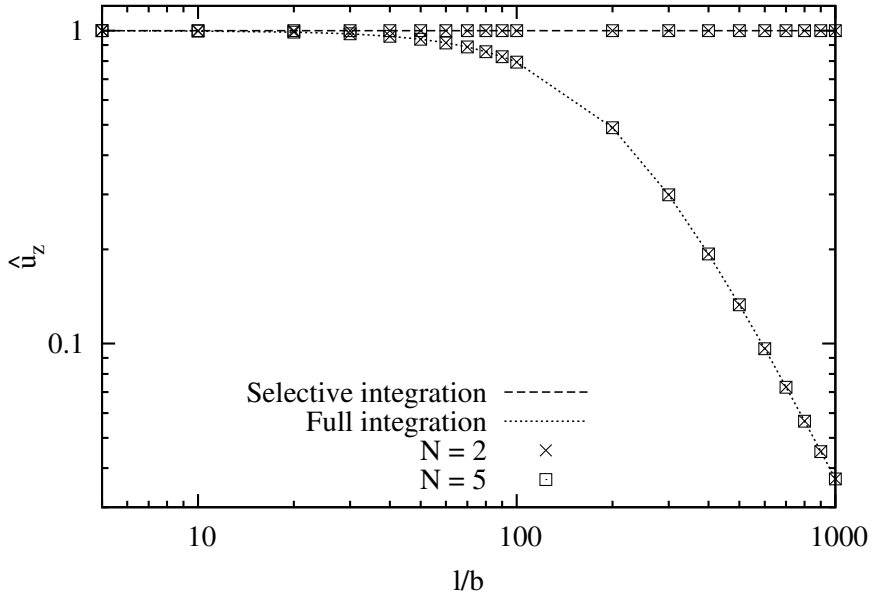

Figure 3: Shear locking correction via selective integration for B2 element, simply supported FGM beam, $n_z = 1$.

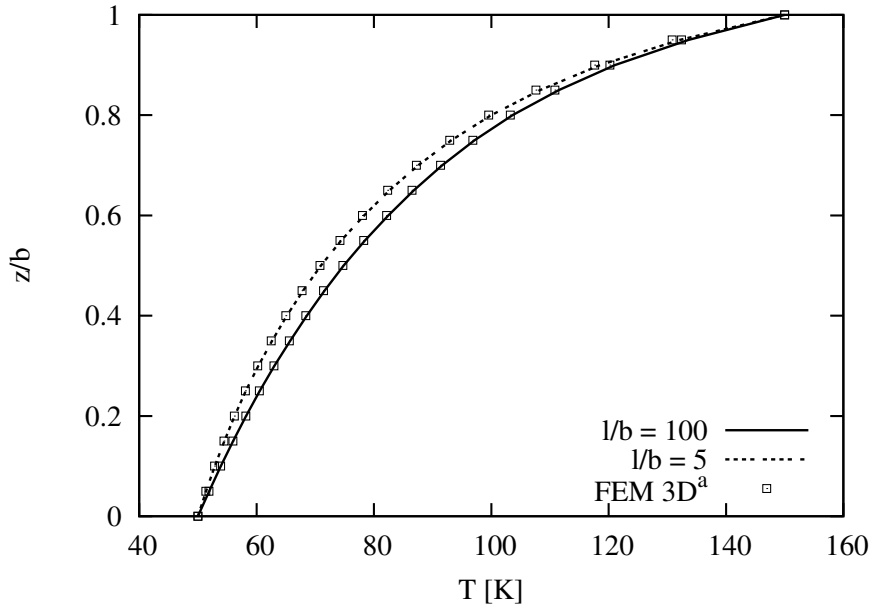

Figure 4: Over-temperature profile $T(z)$ [K] along the thickness at $x = l/2$ for slender and short beams, $n_z = 1$.

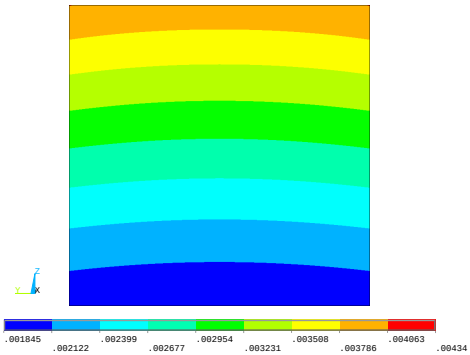

(a) FEM 3D^a, $n_z = 0.5$

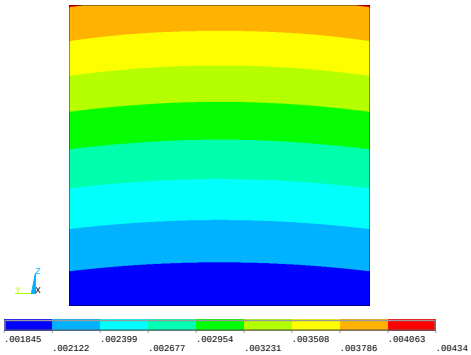

(b) N=13, $n_z = 0.5$

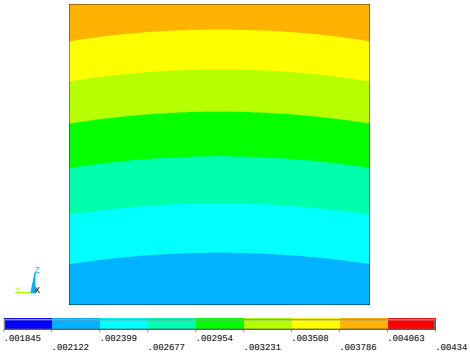

(c) FEM 3D^a, $n_z = 1$

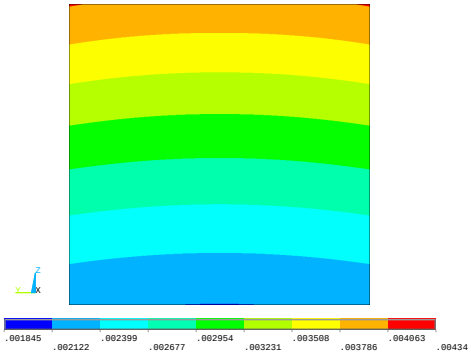

(d) N=13, $n_z = 1$

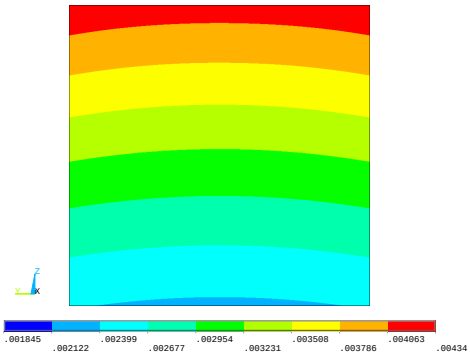

(e) FEM 3D^a, $n_z = 2$

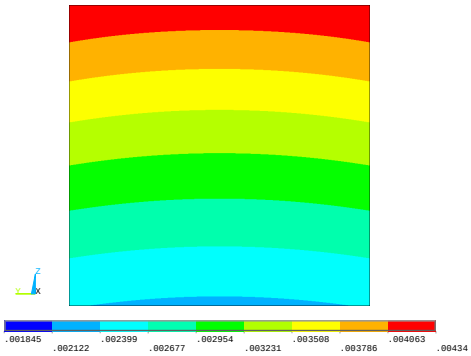

(f) N=13, $n_z = 2$

Figure 5: Axial displacement u_x [m] at $x/l = 1$, cantilever beam, $l/b = 5$.

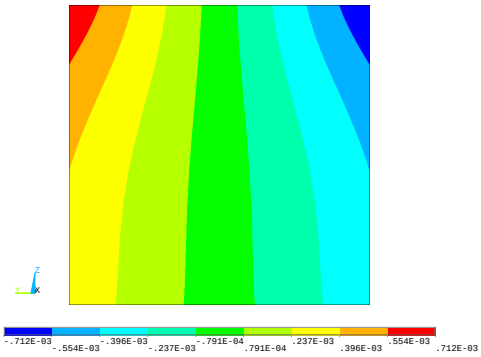

(a) FEM 3D^a, $n_z = 0.5$

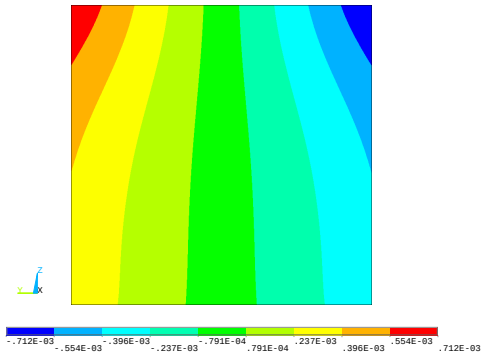

(b) N=13, $n_z = 0.5$

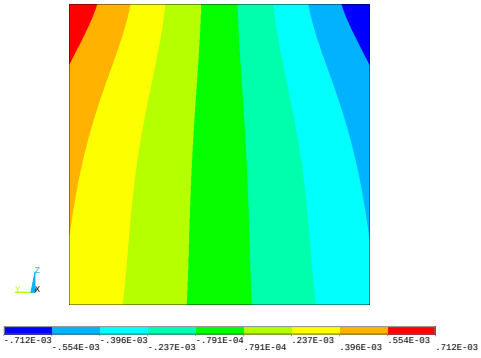

(c) FEM 3D^a, $n_z = 1$

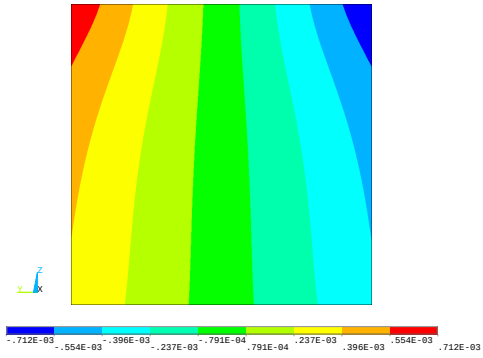

(d) N=13, $n_z = 1$

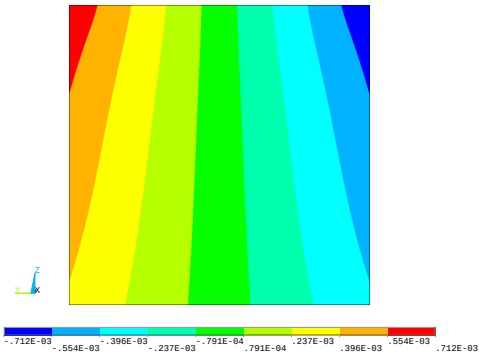

(e) FEM 3D^a, $n_z = 2$

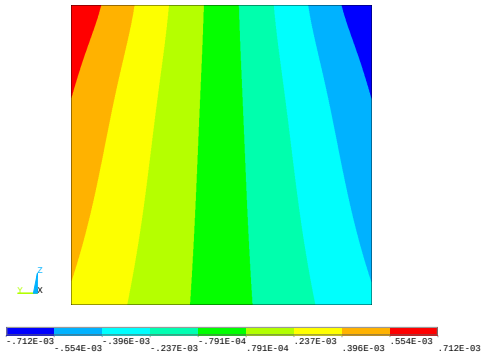

(f) N=13, $n_z = 2$

Figure 6: Through-the-width displacement u_y [m] at $x/l = 1$, cantilever beam. $l/b = 5$.

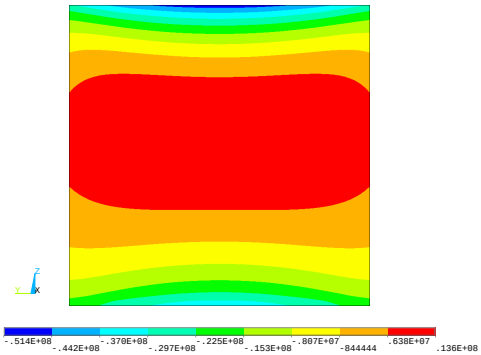

(a) FEM 3D^a, $n_z = 0.5$

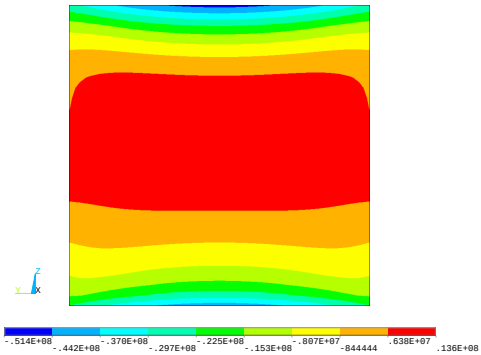

(b) N=13, $n_z = 0.5$

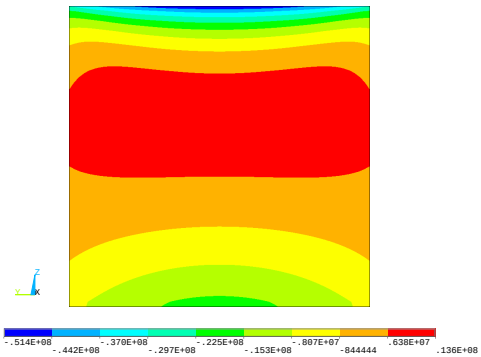

(c) FEM 3D^a, $n_z = 1$

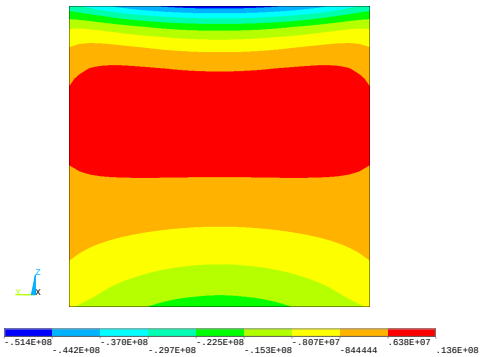

(d) N=13, $n_z = 1$

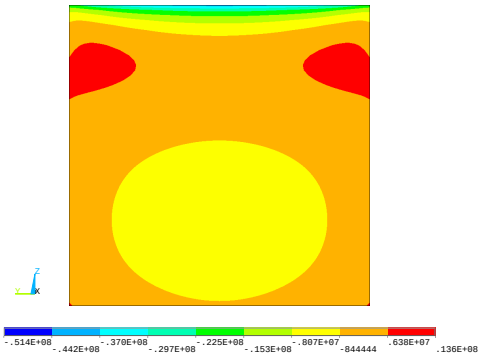

(e) FEM 3D^a, $n_z = 2$

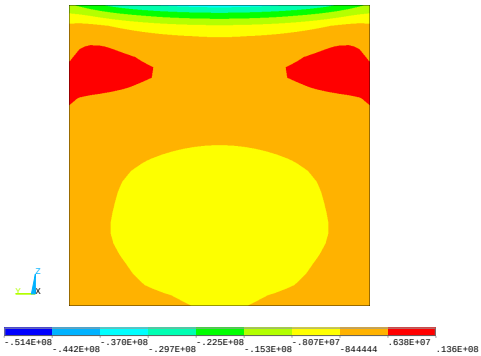

(f) N=13, $n_z = 2$

Figure 7: Axial stress σ_{xx} [Pa] at $x/l = 1/2$, cantilever beam, $l/b = 5$.

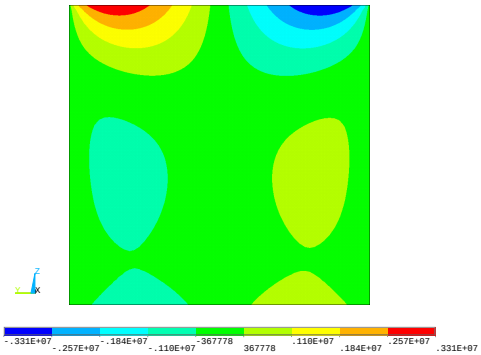

(a) FEM 3D^a, $n_z = 0.5$

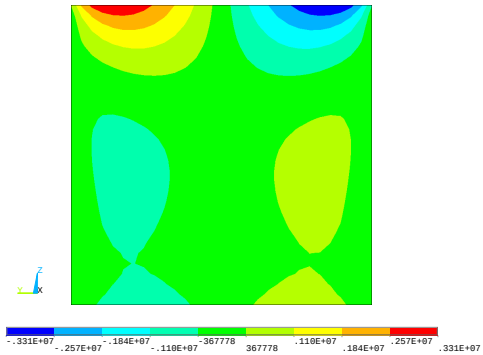

(b) N=13, $n_z = 0.5$

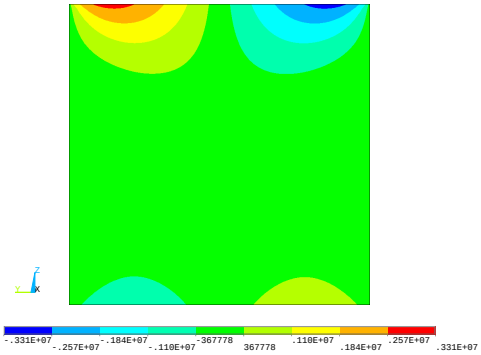

(c) FEM 3D^a, $n_z = 1$

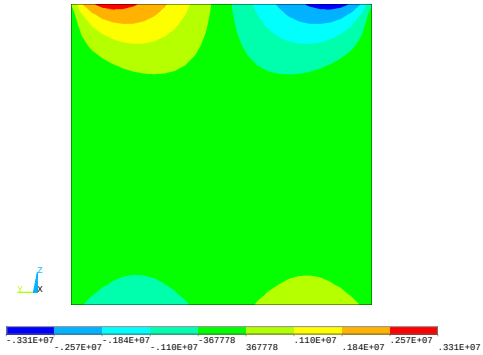

(d) N=13, $n_z = 1$

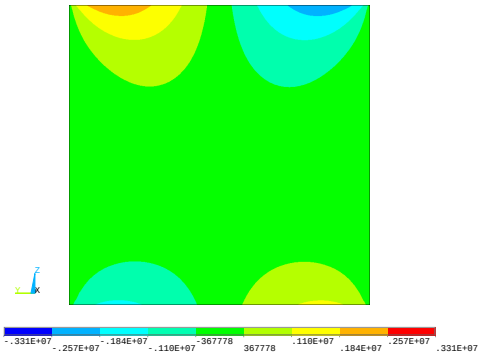

(e) FEM 3D^a, $n_z = 2$

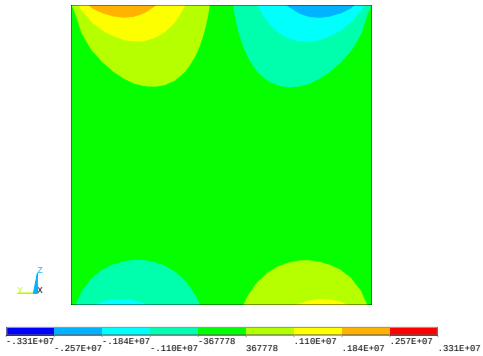

(f) N=13, $n_z = 2$

Figure 8: Shear stress σ_{xy} [Pa] at $x/l = 1/4$, cantilever beam, $l/b = 5$.

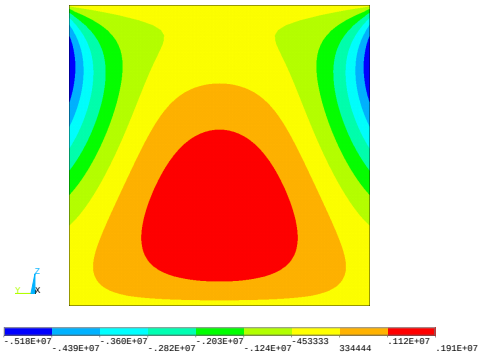

(a) FEM 3D^a, $n_z = 0.5$

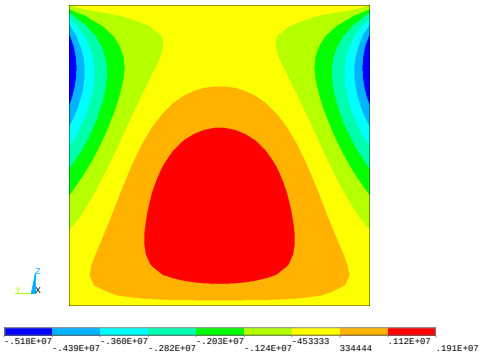

(b) N=13, $n_z = 0.5$

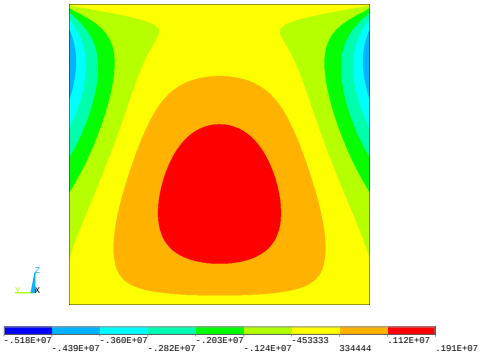

(c) FEM 3D^a, $n_z = 1$

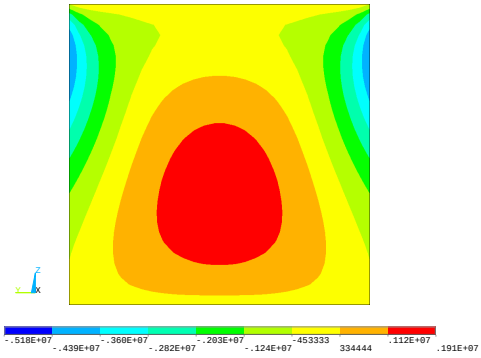

(d) N=13, $n_z = 1$

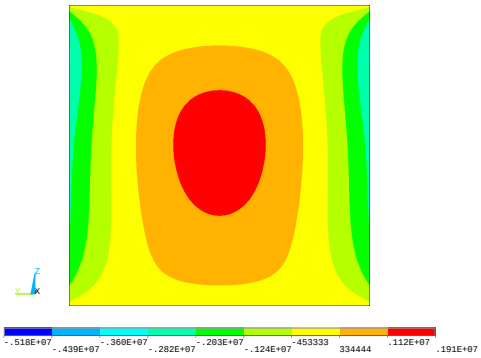

(e) FEM 3D^a, $n_z = 2$

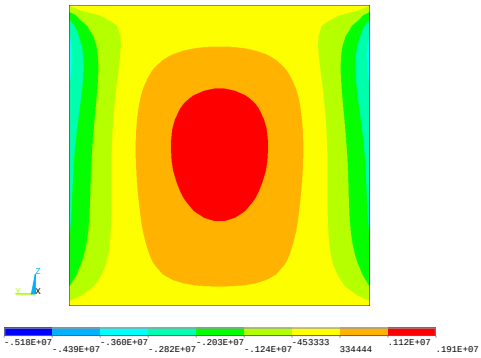

(f) N=13, $n_z = 2$

Figure 9: Shear stress σ_{xz} [Pa] at $x/l = 1/4$, cantilever beam, $l/b = 5$.

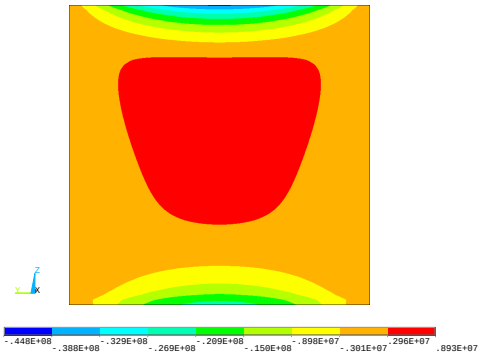

(a) FEM 3D^a, $n_z = 0.5$

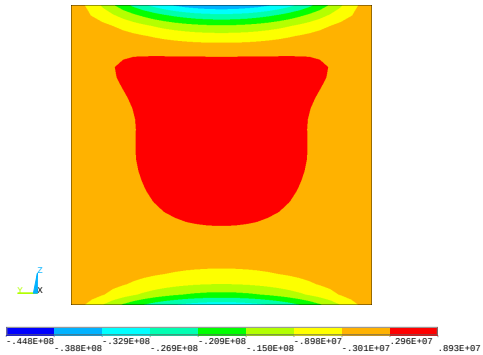

(b) N=13, $n_z = 0.5$

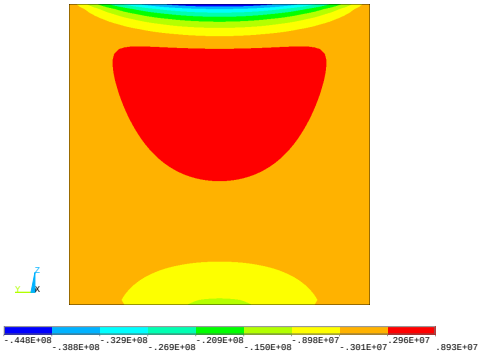

(c) FEM 3D^a, $n_z = 1$

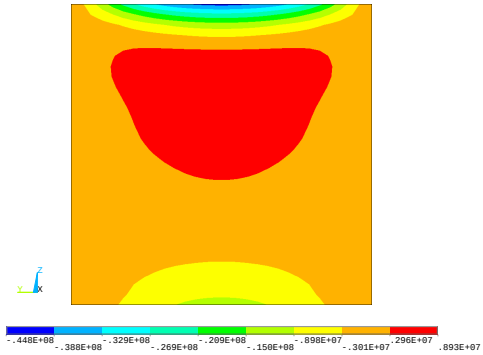

(d) N=13, $n_z = 1$

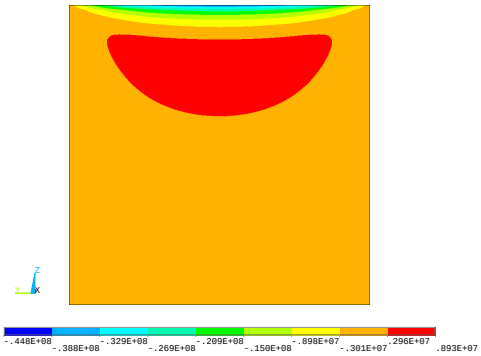

(e) FEM 3D^a, $n_z = 2$

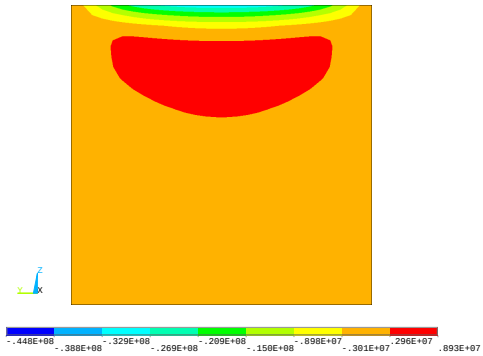

(f) N=13, $n_z = 2$

Figure 10: Through-the-width normal stress σ_{yy} [Pa] at $x/l = 1/2$, cantilever beam, $l/b = 5$.

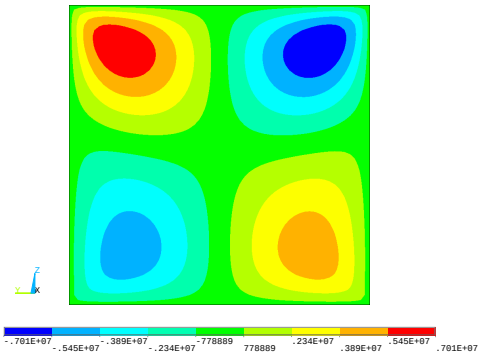

(a) FEM 3D^a, $n_z = 0.5$

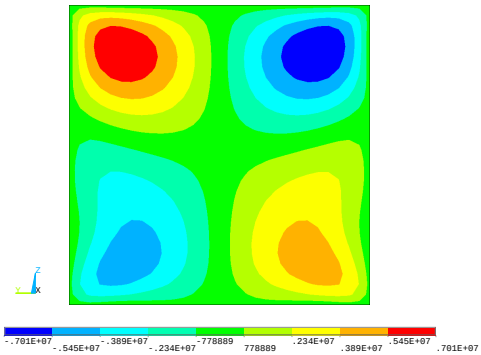

(b) N=13, $n_z = 0.5$

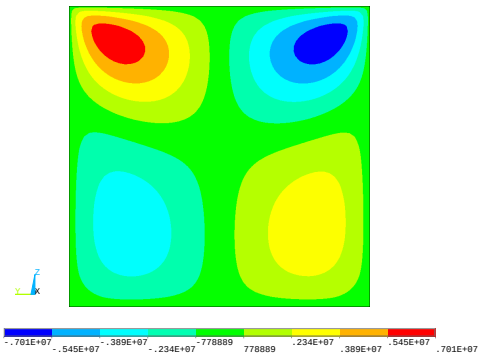

(c) FEM 3D^a, $n_z = 1$

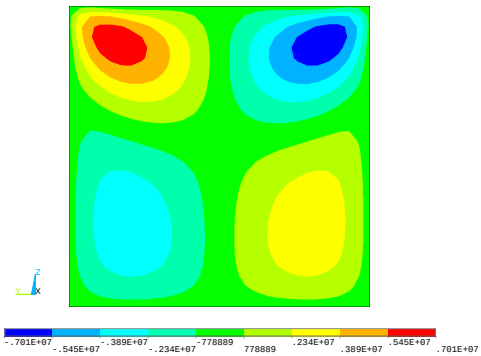

(d) N=13, $n_z = 1$

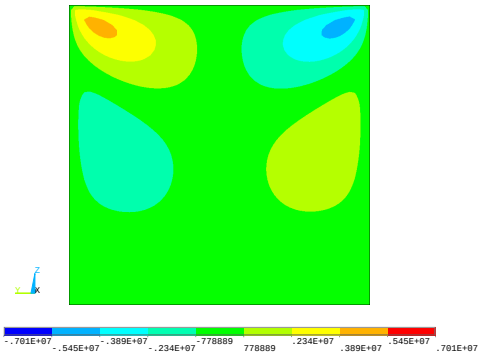

(e) FEM 3D^a, $n_z = 2$

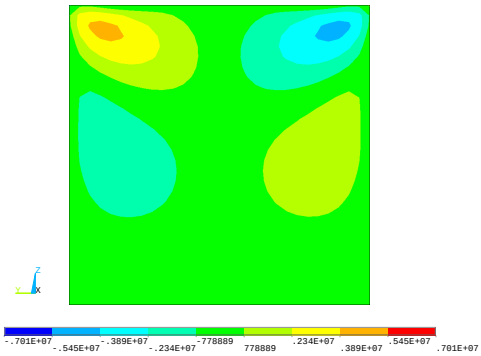

(f) N=13, $n_z = 2$

Figure 11: Shear stress σ_{yz} [Pa] at $x/l = 1/2$, cantilever beam, $l/b = 5$.

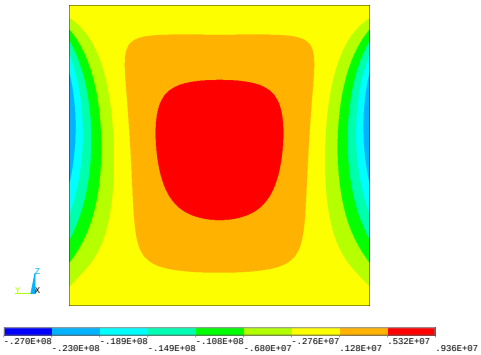

(a) FEM 3D^a, $n_z = 0.5$

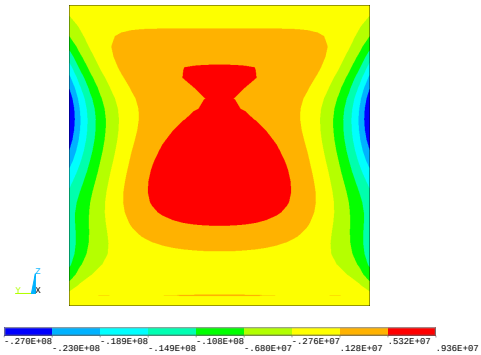

(b) N=13, $n_z = 0.5$

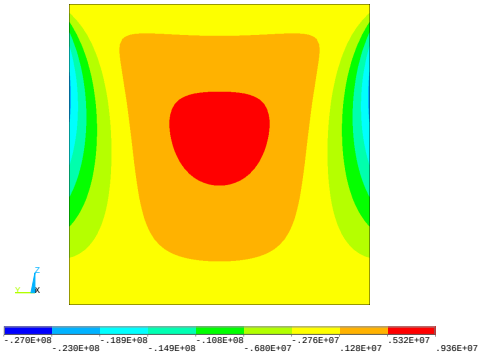

(c) FEM 3D^a, $n_z = 1$

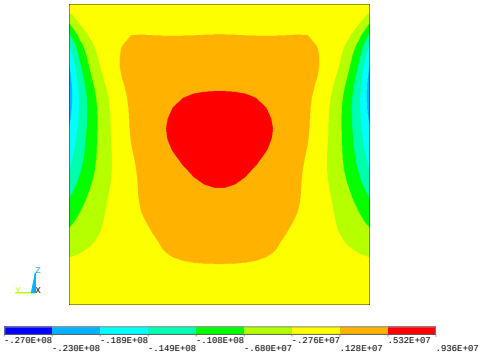

(d) N=13, $n_z = 1$

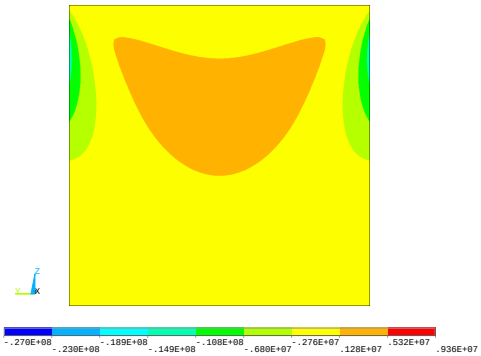

(e) FEM 3D^a, $n_z = 2$

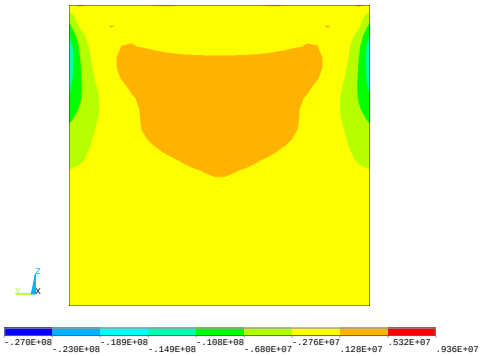

(f) N=13, $n_z = 2$

Figure 12: Through-the-thickness normal stress σ_{zz} [Pa] at $x/l = 1/2$, cantilever beam, $l/b = 5$.